Ceramics International 47 (2021) 26947–26954

Contents lists available at ScienceDirect

Ceramics International

journal homepage: www.elsevier.com/locate/ceramint

Pure perovskite $BiFeO_3$–$BaTiO_3$ ceramics prepared by reaction flash sintering of Bi_2O_3–Fe_2O_3–$BaTiO_3$ mixed powders

Ahmed Taibi [a,b], Salem Chaguetmi [a], Pedro E. Sánchez-Jiménez [b,c,**], Antonio Perejón [b,c,*], José Eduardo García [d], Hamid Satha [a], Luis A. Pérez-Maqueda [b]

[a] Laboratoire LSPN, Université 8 Mai 1945 Guelma, BP 401, Guelma, 24000, Algeria
[b] Instituto de Ciencia de Materiales de Sevilla, C. S. I. C.-Universidad de Sevilla, C. Américo Vespucio No 49, 41092, Sevilla, Spain
[c] Departamento de Química Inorgánica, Facultad de Química, 41012, Universidad de Sevilla, Sevilla, Spain
[d] Department of Physics, Universitat Politècnica de Catalunya, 08034, Barcelona, Spain

ARTICLE INFO

Keywords:
$0.67BiFeO_3$-$0.33BaTiO_3$
Reaction flash-sintering
Current limit
Flash sintering

ABSTRACT

In this work, the $0.67BiFeO_3$-$0.33BaTiO_3$ ferroelectric ceramic was prepared by Reaction Flash Sintering (RFS). This preparation technique combines synthesis and sintering in a single Flash experiment. The starting oxides reacted during the flash to produce a stoichiometric well-sintered solid solution at a temperature of 858 °C by applying a modest field of 35 V cm^{-1}. The process takes place in a matter of seconds, which allows obtaining a pure perovskite structure without secondary phases. X-ray diffraction (XRD) results show the mixture of rhombohedral and pseudocubic phases expected for a composition that lies within a morphotropic phase boundary (MPB) region, since a significant splitting is observed in the reflections at 2θ values of 39° and 56.5°. The microstructure exhibit a peculiar bimodal grain size distribution that determines the electrical properties. As compared with previous results, flash-prepared $0.67BiFeO_3$-$0.33BaTiO_3$ evidences smaller grain size, as well as slightly lower remanent polarization (P_r) and smaller coercive field (E_c) under similar electric fields. It is also demonstrated that the preparation by RFS provides benefits regarding electrical energy consumption.

1. Introduction

Bismuth iron oxide, $BiFeO_3$ (BFO), is a lead free multiferroic material that has received extensive attention due to its high Curie temperature (Tc ~ 830 °C) and its attractive polarization (Ps ~ 100 μC/cm^2) [1–3]. However, the main problem of the single-phase BFO system is its high leakage current and low piezoelectric performance [4,5], which limits its practical applications in devices. It is well known that the combination between BFO and other ABO_3 perovskite systems significantly improves the piezoelectric properties [6–8]. ABO_3-modified BFO ceramics, such as the $(1-x)BiFeO_3$-$xBaTiO_3$ (BFO-BT) system near the morphotropic phase boundary (MPB) have attracted extensive attention as a new generation of lead-free piezoelectric ceramics because of its promising piezoelectric performance, high Tc and reduced leakage current (T_C > 400C) [6,9,10]. Basically, dense $BiFeO_3$–$BaTiO_3$ ceramics are synthesized in two steps, including preparation and sintering of $BiFeO_3$–$BaTiO_3$ powders. Both steps need high temperatures and long treatment times, which are high energy consuming. Under such conditions, it is difficult to prepare dense and stoichiometric $BiFeO_3$–$BaTiO_3$ ceramics due to high Bi volatilization and Fe^{3+} reduction that lead to the formation of impurities such as $Bi_2Fe_4O_9$, $Bi_{25}FeO_{39}$, or Bi_2O_3 [11–14]. Thus, other techniques to prepare dense and stoichiometric $BiFeO_3$–$BaTiO_3$ ceramics are required.

Since it was first reported in 2010 [15], flash sintering has attracted the attention of many researchers for several reasons, including its lower onset sintering furnace temperatures and its short time densification as compared to conventional preparation techniques [16–22]. Also, it is a promising processing method to prevent the high volatility of certain elements during the preparation of materials, such as potassium [23], bismuth [24–27] and lithium [28]. Moreover, it has been reported that it is possible to prepare single-phase oxides in a single step by flash sintering of its precursors [29]. This methodology has been called reaction flash sintering (RFS) and has been used to prepare other materials, such as lead zirconate titanate (PZT), sodium potassium niobate (KNN) and other multi-phase oxide ceramics [23,30–33]. To the best of our knowledge, there are no report on the preparation of $BiFeO_3$–$BaTiO_3$

* Corresponding author. Instituto de Ciencia de Materiales de Sevilla, C. S. I. C.-Universidad de Sevilla, C. Américo Vespucio no 49, 41092, Sevilla, Spain.
** Corresponding author. Departamento de Química Inorgánica, Facultad de Química, 41012, Universidad de Sevilla, Sevilla, Spain.
E-mail addresses: pedro.enrique@icmse.csic.es (P.E. Sánchez-Jiménez), antonio.perejon@icmse.csic.es (A. Perejón).

https://doi.org/10.1016/j.ceramint.2021.06.108
Received 26 April 2021; Received in revised form 11 June 2021; Accepted 14 June 2021
Available online 17 June 2021

ceramics using reaction flash sintering.

In this work, the preparation of $0.67BiFeO_3$-$0.33BaTiO_3$ (abbreviated as BFO-33BT) is investigated using the reaction flash sintering method. In BFO-33BT, the $BaTiO_3$ molar fraction (33%) was chosen since it is located in the morphotropic phase boundary (MPB) range [34]. Compositions where x is in the range 0.25–0.35 lie near a morphotropic phase boundary (MPB), exhibiting rhombohedral and pseudocubic phases simultaneously [3,14,35]. The starting powders reacts during the flash to produce a well-sintered stoichiometric ceramic, with a peculiar microstructure.

2. Materials and methods

High purity oxides, Bi_2O_3 (Sigma-Aldrich, 99.9%), Fe_2O_3 (Sigma-Aldrich, 99%) and $BaTiO_3$ (Sigma-Aldrich, 99%), were used in the stoichiometric ratio for the preparation of $0.67BiFeO_3$-$0.33BaTiO_3$ (BFO-33BT) by RFS method. Stoichiometric amounts of the starting oxides were ball milled for 15 min in a planetary ball-mill with the objective of obtaining a homogeneous mixture. Approximately 900 mg of the powders mixture were pressed into dog-bone shaped specimens under a pressure of 500 MPa. In order to provide good contact sample-electrodes, platinum paste was added into the holes of the handles of the green-body dog-bones. The distance between the electrodes was 2 cm. The electrode wires were connected to a 1500 W DC power supply (EA-PSI 9750–06 DT). Current and voltage input signals were measured using a Keithley 2110 multimeter. The flash event was held for 30 s and the adjustment of the experimental flash conditions (applied electric field (E) and current density limit (I)) was carried out according to the protocol described in a previous work [36]. The XRD measurements were performed in a Rigaku MiniFlex diffractometer, using Cu K_α radiation with a scan rate of 0.02°/s in the 15°–70° 2θ range. Raman spectra was measured at room temperature using a Horiva Jobin Yvon LabRam HR800 microscope with a green laser excitation of 532 nm, and the fitting of the spectra was carried out using a Gaussian function. The density of the BFO-33BT flashed samples was determined using the Archimedes method. Morphological and compositional characterization was investigated by scanning electron microscopy (Hitachi S-4800), connected with an energy dispersive X-ray spectrometer (EDX).

Silver electrodes were painted on parallel polished faces of the samples for electrical measurements. The impedance measurements were performed in a 360–440 °C temperature range and over the frequency range 100 Hz-1 MHz, using a Newtons4th Ltd Impedance analysis interface (PSM1735 NumetriQ). The dielectric characterization was performed in disc-shaped unpoled samples using an Agilent E4980A Precision LCR Meter, the real ε′ and imaginary ε'' parts of the permittivity being measured at several frequencies between 100 Hz and 1 MHz. Samples were placed in a programmable tubular oven for measurement in a temperature range from room temperature to 600 °C. Electric field-induced polarization (P-E) hysteresis loops were measured in a typical Sawyer-Tower configuration by applying a sinusoidal electric field of amplitude of 60 kV cm^{-1} at a frequency of 1 Hz, using a Hewlett-Packard 33120A signal generator and a Trek 663 signal amplifier, at room temperature. The electric field-induced macroscopic strain was measured by adding a WayCon inductive position transducer conditioning with a Solartron OD5 Module to the P-E setup. Samples were then poled in a silicone bath at 80 °C under a dc electric field of 60 kV cm^{-1} for 30 min, and subsequently aged for two days before measurements were taken in order to prevent the influence of aging processes. The static longitudinal direct piezoelectric constant was obtained by using a KFC Technologies PM3500 d_{33}-m.

3. Results and discussion

3.1. Preparation of BFO-33BT by reaction flash sintering

Series of experiments for the preparation of $0.67BiFeO_3$-$0.33BaTiO_3$ by reaction flash sintering were performed with the aim of optimizing the experimental conditions, i.e., applied electric field and selected current density limit. The results obtained from these experiments are displayed in Fig. 1. In this figure, Fig. 1(a), two large regions where reaction is either incomplete or heterogeneous (due to localization of the electrical current) can be clearly distinguished. Thus, only in a very narrow range of experimental conditions (electric field of 35 V cm^{-1} and current density of 60 or 70 mA mm^{-2}), within the boundary between incomplete and heterogeneous regions, the reaction is optimal, yielding a homogeneous material. The corresponding captured images of resulting flash sintered samples corresponding to incomplete, heterogeneous and optimal reactions are also included in Fig. 1(b–d). Samples prepared within the optimal experimental conditions range yielded an identical density of 6.90 g cm^{-3}, corresponding to a relative density of 91%, as determined by the Archimedes method. Therefore, an electric field of 35 V cm^{-1} and a current density of 60 mA mm^{-2} can be considered as the best conditions for the preparation of BFO-33BT by reaction flash sintering, as a lower power density (0.210 W mm^{-3}) is required as compared to the other sample obtained with a current intensity of 70 mA mm^{-2} (0.245 W mm^{-3}).

Fig. 2 shows the evolution of electric field, current intensity and dissipated power as a function of the furnace temperature for the reaction flash sintering experiment at an electric field of 35 V cm^{-1} and a current density limit of 60 mA mm^{-2}. The three stages of the flash sintering experiment are clearly observed in these figures. Thus, after a first stage, where the electric field is maintained constant by the power supply at 35 V cm^{-1}, the current density (Fig. 2(a)) rise sharply in a second stage to the preset maximum value of 60 mA mm^{-2} (corresponding to a power dissipation of 210 mW mm^{-3}, Fig. 2(b)). At this point, the power supply shifts from constant voltage (CV) to current controlled (CC) regime. In the third stage, the sample is maintained in a flash-activated state under controlled current (CC). The onset of flash is reached at a furnace temperature of 858 °C. The temperature of the sample at stage III of the flash can be estimated by using the blackbody radiation model [37]:

$$T = \left[T_0^4 + \frac{W}{A\varepsilon\sigma}\right]^{1/4} \quad (1)$$

where T and T_0 respectively reflect the real sample temperature and the furnace temperature, W is the power dissipation, A is the surface area of

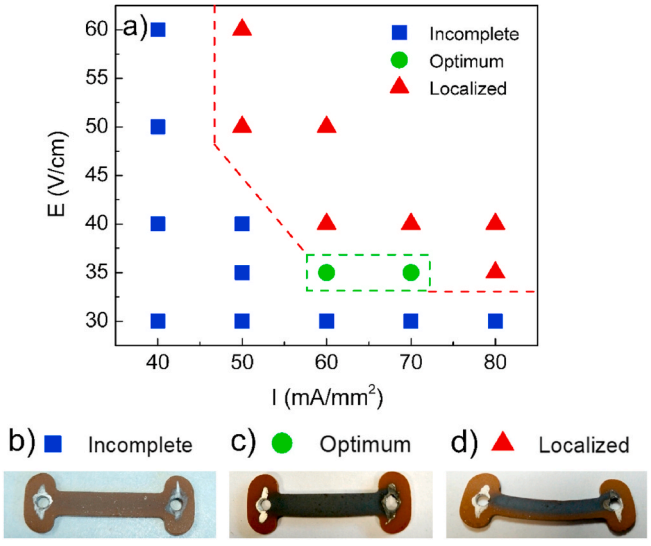

Fig. 1. (a) Experimental conditions used for the reaction flash sintering of BFO-33BT. Dog bone samples for (b) incomplete reaction (40 V cm^{-1}, 40 mA mm^{-2}), (c) optimum reaction conditions (35 V cm^{-1}, 60 mA mm^{-2}) and (d) heterogeneous reaction (due to localization, 50 V cm^{-1}, 60 mA mm^{-2}).

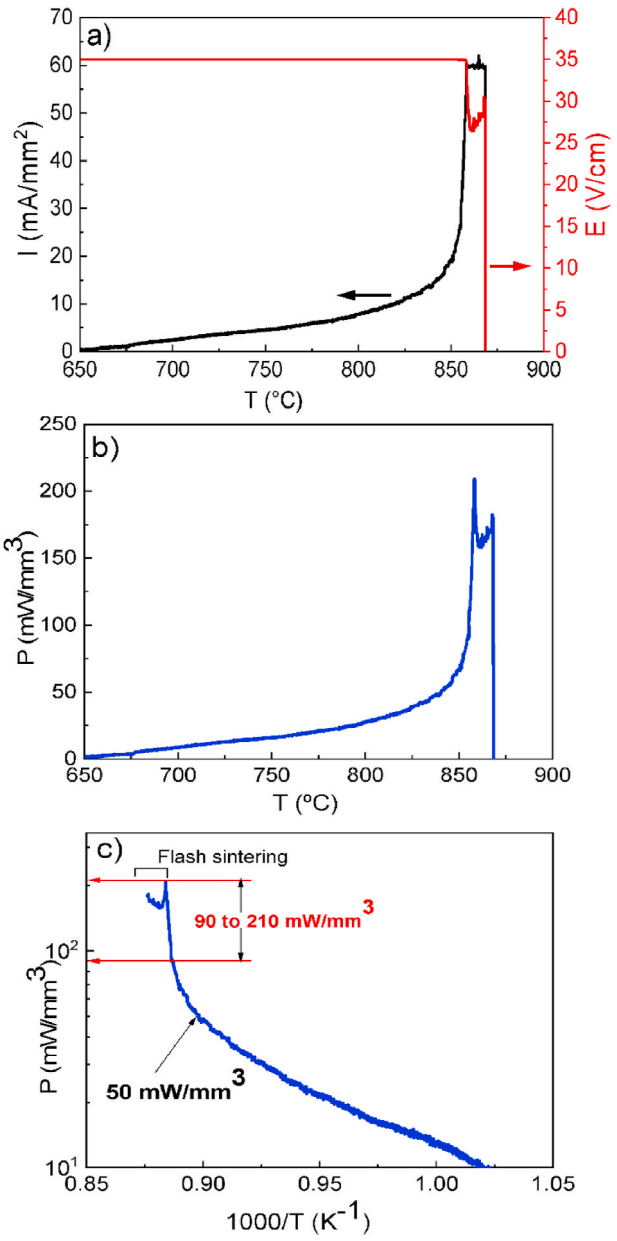

Fig. 2. (a) Evolution of electric field and current density, and (b) power dissipation versus furnace temperature for the reaction flash sintering experiment performed at an electric field of 35 V cm^{-1} and a current density limit of 60 mA mm^{-2}. (c) Arrhenius plot for the BFO-33BT flashed sample.

the sample (m^2), ε is the emissivity (0.9) and σ is Stefan's constant (5.67×10^{-8} W m^{-2} K^{-4}). Thus, the estimated real temperature of the sample was found to be approximately 1050 °C.

Field-assisted processing of materials is commonly analyzed in terms of power dissipation density. The Arrhenius plot of the power dissipation is shown in Fig. 2(c). At low temperatures, the power dissipation exhibits a linear-like type behavior. This behavior is interrupted at 50 mW mm^{-3} when the flash event takes place, followed by a sharp increase in the 90–210 mW mm^{-3} power dissipation range that signals the onset of flash. It is remarkable that the inflexion of the curve that signals the flash event occurs within the same narrow range (10–50 mW mm^{-3}) described in literature for flash sintering of numerous materials, despite the fact that, in this case, there is reaction and sintering taking place at the same time [38].

Fig. 3 shows the room temperature XRD pattern of the BFO-33BT sample before and after the flash (at 35 V cm^{-1} and 60 mA mm^{-2}).

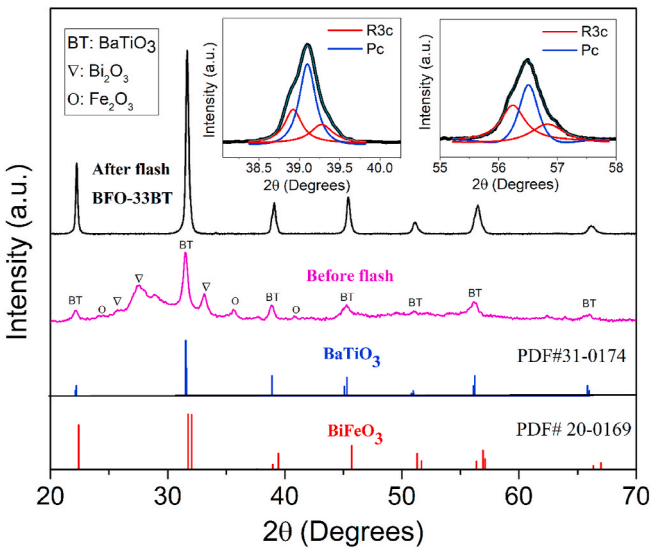

Fig. 3. XRD patterns of BFO-33BT sample before and after the reaction flash process.

The JCPDS (Joint Compounds Powder Diffraction Standards) cards of $BiFeO_3$ and $BaTiO_3$ are also listed in Fig. 3. The XRD peaks of the sample before the flash are broad due to the small crystallites size obtained after ball milling during 15 min and the mixture is completely composed of the starting precursors: Bi_2O_3 (JCPDS #71–0465), Fe_2O_3 (JCPDS # 24–0072) and $BaTiO_3$ (JCPDS #31–0174). After the flash, the XRD pattern of the sample evidences that the composition BFO-0.33BT is within the MPB region of the BFO-BT system. Thus, a significant splitting is observed in the reflections at 2θ values of 39° and 56.5° (see inset in Fig. 3), which has been associated with the coexistence of rhombohedral (R3c) and pseudocubic (PC) phases [14,39,40]. The ratio between the R3c and PC phases was estimated by deconvolution of these reflections, using a pseudo-Voigt function, and the results indicate that a mixture of 57% R3c and 43% PC phases is obtained. Thus, it can be concluded that the Bi_2O_3–Fe_2O_3–$BaTiO_3$ mixed powders are transformed to a mixture of R3c and PC phases of 0.67BiFeO3-0.33BaTiO3 after the reaction flash sintering.

The presented synthesis route using reaction flash sintering led to a significant reduction of the furnace reaction temperature (Ts ~ 858 °C) and time (t = 30s) for $0.67BiFeO_3$-$0.33BaTiO_3$, compared to conventional solid-state method [6,9,41], which requires at least 980 °C and 2–3 h of dwell time.

The Raman spectrum for the BFO-33BT sample obtained under optimal conditions (35 V cm^{-1}, 60 mA mm^{-2}) is shown in Fig. 4. The spectrum obtained clearly presents 8 mode peaks, three of them belonging to A_1 modes at 177, 250 and 476 cm^{-1}, and five to E modes at 307, 522, 566, 663 and 750 cm^{-1}. These values are consistent with previous reports of $BiFeO_3$–$BaTiO_3$ based ceramics. Thus, Bouzidi et al. [42], Qi et al. [43] and Li et al. [44] observed, for conventionally prepared $BiFeO_3$–$BaTiO_3$, bands at approximately the same values as for the A_1 and E modes. They were able to distinguish two main regions in the Raman spectrum: (i) low frequency vibrational modes below 400 cm^{-1}, which are essentially associated to the vibrations of B–O band. In particular, the most intense vibration mode, at around 250 cm^{-1}, has been assigned to Fe/Ti–O. (ii) High frequency vibrational modes above 400 cm^{-1} reflect to the vibrational frequencies of BO_6 octahedral. Our results are also in good agreement with those obtained by Pakalniškis et al. [35] for $BiFeO_3$–$BaTiO_3$ samples prepared by sol gel method. On the other hand, the appearance of the vibration mode at around 750 cm^{-1} indicates the existence of the rhombohedral (R3c) symmetry [42], which confirms the mixture of rhombohedral and pseudocubic symmetry expected at the MPB region.

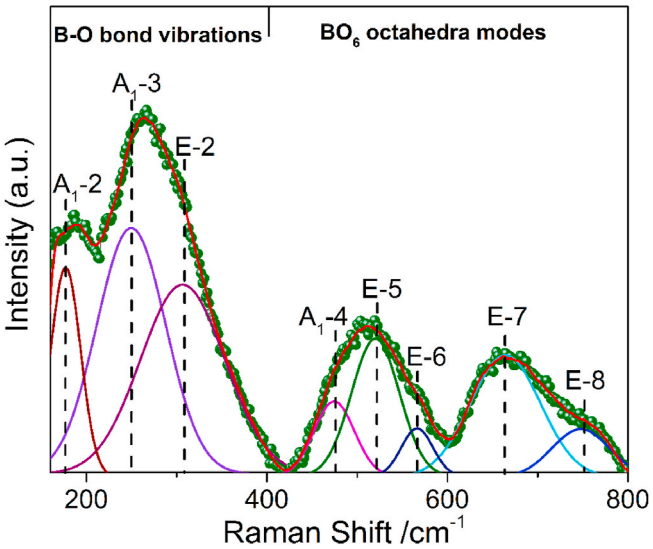

Fig. 4. Raman spectrum for the BFO-33BT sample obtained under optimal conditions (Fig. 3(c)).

The surface morphology of the fracture of BFO-33BT reaction flash sintered sample, as observed by SEM, is shown in Fig. 5(a). It corresponds to a well sintered material with a small amount of pores. Fig. 5(b) shows a high-magnification SEM image of the fractured surface. It shows a peculiar microstructure with a bimodal grain size distribution, where small grains are located in the grain boundaries between larger grains. The mean value corresponding to the large grains is 3.4 ± 1 μm, while the mean value corresponding to the smaller grains is 0.4 ± 0.1 μm. The EDS mapping shows that Bi, Fe, Ba and Ti are uniformly dispersed within the flashed sample, both small and large grains show identical compositional ratios, confirming the chemical homogeneity of the BFO-33BT ceramic sample (Fig. 5(c–g)).

3.2. *Dielectric and impedance spectroscopy of BFO-33BT flashed sample*

The dielectric properties of the BFO-33BT flashed sample were studied as a function of temperature at selected frequencies and plotted in Fig. 6. Both the dielectric permittivity (Fig. 6(a)) and dielectric loss (Fig. 6(b)) appeared to increase clearly at temperatures above 200 °C, especially when measured at low frequencies. These effects are due to the increase of the electrical conductivity of the BFO-33BT flashed sample and to the associated space-charge polarization [45,46]. Thus, an extrinsic contribution to the dielectric permittivity due to the high dielectric loss is expected. A frequency-dependent dielectric anomaly appears slightly over 400 °C that can be attributed to the ferroelectric-paraelectric transition. The dielectric permittivity decreases and the peak shifts to higher temperatures with increasing frequencies. The strong dependence of the dielectric permittivity (ε_r) on frequency and the diffuse phase transition (Tc ~ 440 °C), suggests a relaxation phase transition behavior. This confirms previous finding by Singh et al. [47] having observed a relaxor-type ferroelectric behavior

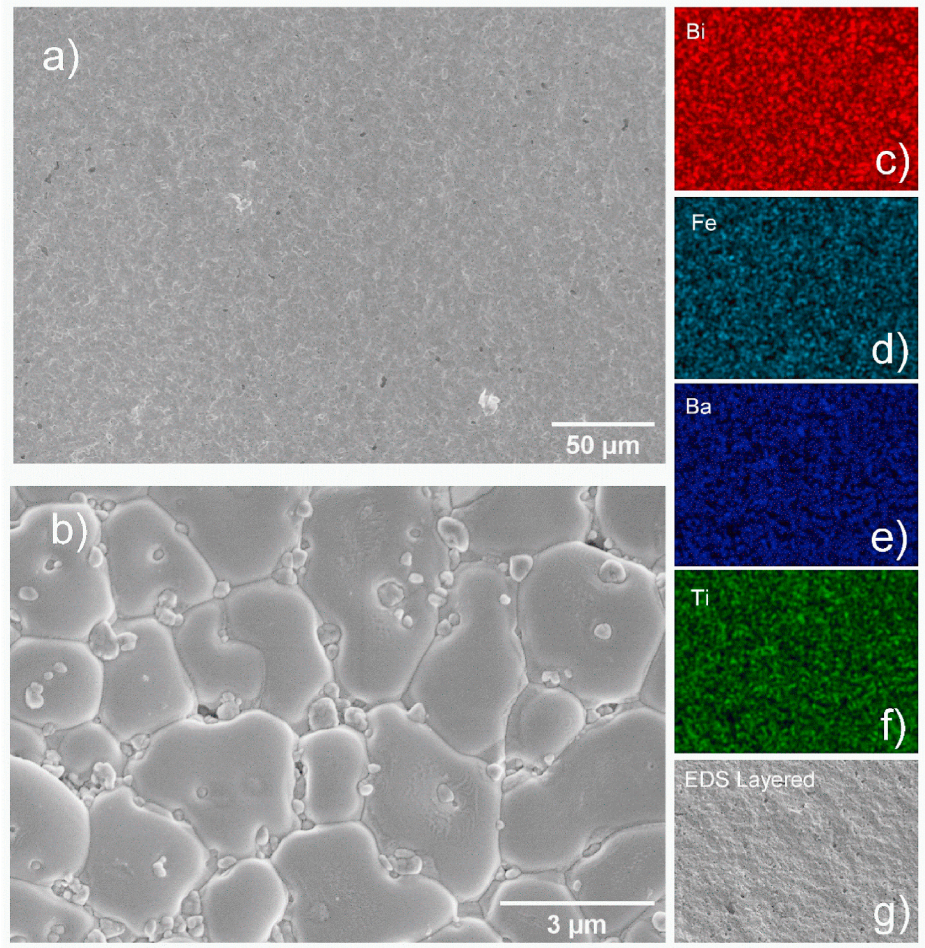

Fig. 5. SEM micrographs of BFO-33BT obtained under optimal conditions (a) surface morphology of the fracture surface, (b) SEM image at high magnification. EDS elemental mapping of (c) Bi, (d) Fe, (e) Ba, (f) Ti and (g) EDS layered image.

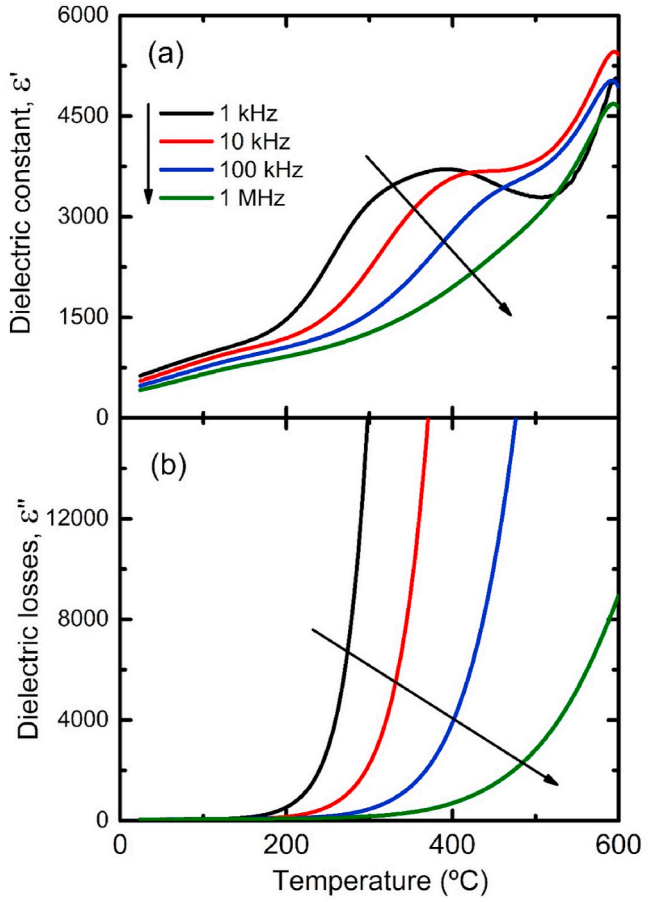

Fig. 6. Temperature dependent (a) permittivity and (b) loss for BFO–33BT obtained by reaction flash sintering.

for samples prepared using $BaTiO_3$ as starting precursor. The dielectric loss significantly shifts to higher temperatures at higher frequencies, thereby suggesting mobile ions or vacancies might constitute the main conduction mechanism. Overall, the observed properties are consistent with previous reports [3,14,34,48].

In order to check the electrical homogeneity of the BFO-33BT flashed sample, impedance spectroscopy measurements were performed. Impedance data for BFO-33BT in air are displayed in Fig. 7. The Nyquist plot of BFO-33BT flashed sample is presented in Fig. 7(a). The flashed sample exhibits typical single semicircular arcs at all temperatures. As the temperature increases, the intercept of the semicircles on the Z' axis is smaller, indicating a decrease in the resistivity of the BFO-33BT sample. Fig. 7(b) shows the Arrhenius plots of the conductivity for BFO–33BT. The average activation energy value, Ea, obtained from the plot slope, is found to be equal to 1.10 eV. This Ea value is quite similar to other results found in the literature for $BiFeO_3$–$BaTiO_3$ based ceramics [49–51]. Such value is consistent with reported activation energies of oxygen vacancies ($V_{\ddot{O}}$), suggesting the conduction mechanism relies on oxygen vacancies that dominate the conductivity as elsewhere reported [14,52]. This mechanism can be further promoted by the synthesis method as it has been shown how ceramics prepared by flash sintering exhibit a significant amount of defects and ion vacancies [38,53]. To verify the existence of short-range and long-range ordering in BFO-33BT sample, spectroscopic plots of imaginary components of impedance, Z″, and modulus, M″, are plotted at 380 °C (Fig. 7(c)). As seen from the graph, both peaks are almost in the same position, indicating good electrical homogeneity of BFO-33BT sample. The capacitance increases with increasing temperature (Fig. 7(d)), and it is also noted that at all temperatures the capacitance shows a single capacitance plateau, with an approximate value range of 0.20–0.60 nF cm^{-1}. This indicates the presence of single electrical responses.

3.3. Ferroelectric and piezoelectric properties of BFO-33BT flashed sample

The room-temperature polarization hysteresis loops, measured under 60 kV cm^{-1} at 1 Hz are shown in Fig. 8. The loops exhibit poor saturation what can be attributed to the bimodal microstructure with relatively small grains obtained by reaction flash sintering. The large density of grain boundaries and defects as well as the consequently smaller ferroelectric domains hamper domain switching and limits maximum polarization [54]. The measured P_r, *Ec* and *Smax* are included in Table 1. Fig. 8 also displays the electric-field induced strain curves at 60 kV cm^{-1}. The sample exhibits the symmetric butterfly-shaped loops characteristic of ferroelectric materials. A small maximum strain of 0.034% is measured. All remnant and maximum polarization, as well as maximum strain appear slightly smaller than reported elsewhere, most probably due to the large number of small grains [14,55]. These measured properties are consistent with values reported in previous works [3].

Table 1 also include the values of d_{33}, ε' and ε'' at room temperature. The measured piezoelectric constant d_{33} is 30 pC/N. The small value is a consequence of the low P_r, what hampers the piezoelectric properties.

3.4. Comparison between electrical energy consumption in RFS and conventional preparation

A comparison of the electrical energy consumption during RFS and conventional preparation method (CM) of the material was performed (Fig. 9). A power analyzer PPA 1500 (Newtons4th Ltd. (N4L)) was used to measure the power supplied by the temperature controller to the furnace resistance during the entire experiments (heating rates of 5 °C min^{-1}).

In order to compare the energy consumption in RFS experiment with that of the conventional method, the electrical energy consumed in both processing methods was calculated. It was considered that the preparation of BFO-33BT by the conventional preparation method takes place in two stages, including synthesis (~800 °C for 2 h) and sintering (~1000 °C for 3 h) [8,12–14]. Therefore, the total electric energy consumed in the conventional preparation of BFO-33BT is the quantity of energy consumed by the furnace during synthesis and sintering. Regarding the RFS, the energy consumed includes the energy required to heat up the furnace to the onset flash temperature (858 °C) and the energy delivered by the power supply during the flash (see Fig. 2(b)).

Although at a laboratory scale, the results provide a proof of concept according to which the preparation by reaction flash sintering provides benefits regarding the electrical energy consumption. The total value of 788 Wh of electrical energy consumption in case of the experiment performed by RFS shows a decrease of about 82% compared to the electrical energy consumption of 4512 Wh for conventional preparation (Fig. 9).

The experiments also confirmed the basic principles of flash sintering. Thus, energy is transferred directly to the materials, which provide rapid densification (<60 s) at moderate furnace temperatures. During the conventional preparation method, where energy is generated by external heating elements and transferred to the samples via convection, conduction and radiation, 67% of the total electrical energy is consumed in the sintering stage and the rest of 33% is used during the synthesis stage of BFO-33BT.

4. Conclusions

In this work, $0.67BiFeO_3$-$0.33BaTiO_3$ ceramic specimens have been synthesized and sintered in a single step by means of Reaction Flash Sintering technique. The starting powders, previously mechanically

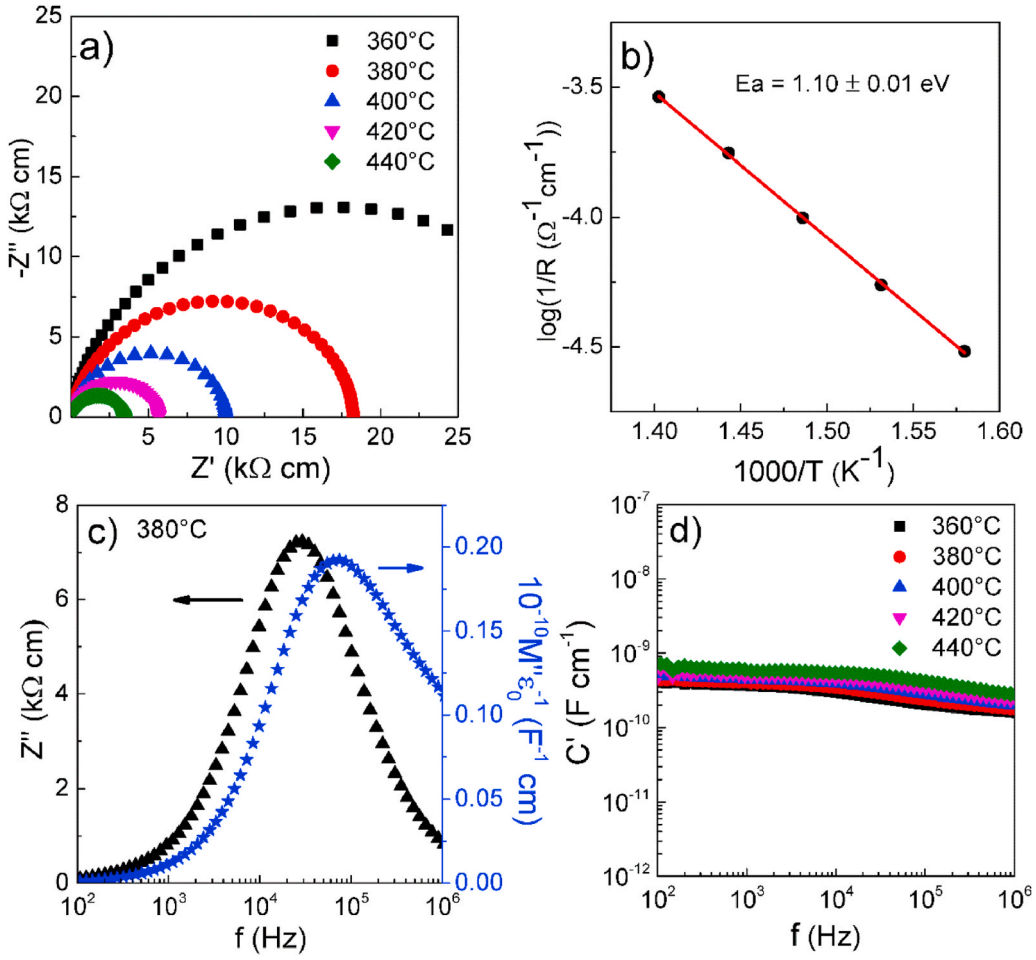

Fig. 7. Impedance data for BFO-33BT obtained by reaction flash sintering: (a) Nyquist plot, (b) Arrhenius plot of total electrical conductivity, (c) spectroscopic plots of imaginary components of impedance, Z″, and modulus, M″ at 380 °C and (d) capacitance versus frequency graph.

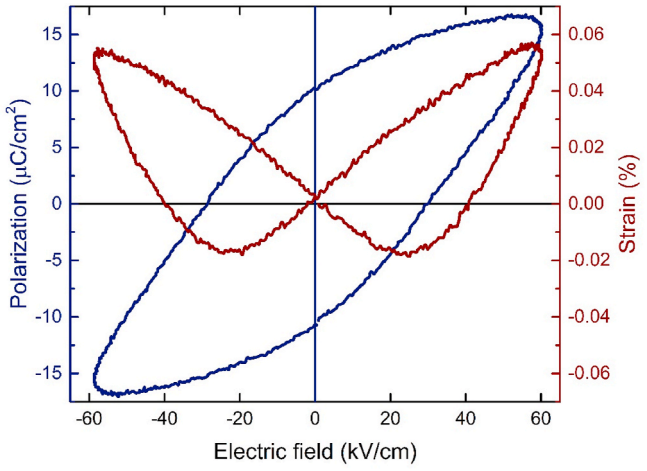

Fig. 8. P–E hysteresis loop and strain curve of BFO-33BT sample prepared by RFS.

mixed to ensure homogeneous distribution, reacted during the flash to produce the stoichiometric solid solution and sintered to near full density in a matter of seconds at a temperature of 858 °C under a modest field of 35 V cm^{-1}. Conversely, conventional solid-state preparation procedures typically require two thermal treatments at temperatures around 1000 °C during hours, what often leads to sample inhomogeneity due to Bi volatilization. Reducing the temperature and length of the preparation method by RFS allows achieving pure perovskite structure without secondary phases nor impurities. With a 33% content in $BaTiO_3$, the structure lies in a MPB region where a rhombohedral R3c phase coexist with a pseudocubic phase. The features of the RFS synthesis method, which greatly reduce the time the material is subjected to high temperatures, lead to a peculiar microstructure of the flashed ceramics. A bimodal grain size distribution with large 3 μm grains coexisting with small 0.4 μm grains is obtained. The electrical properties are largely in line with previous results, what validates RFS as energy and time saving technique for the synthesis and sintering of complex ceramics. Moreover, a comparison of the electrical energy consumption during the RFS and conventional preparation method was performed. It is demonstrated that the energy consumption is almost six times reduced, as compared with the conventional method, when RFS is used for the preparation of the $0.67BiFeO_3$-$0.33BaTiO_3$ ceramic.

Table 1
Remnant polarization (P_r), coercive field (E_c) and strain max (S_{max}) for BFO-33BT prepared by reaction flash sintering. The piezoelectric coefficient (d_{33}), dielectric constant (ε′) and loss (ε′′) at room temperature are also included.

Sample	P_r (μC/cm^2)	E_c (kV/cm)	S_{max} (%)	d_{33} (pC/N)	ε′	ε″
BFO-33BT	3.0	24	0.034	30	620	0.07

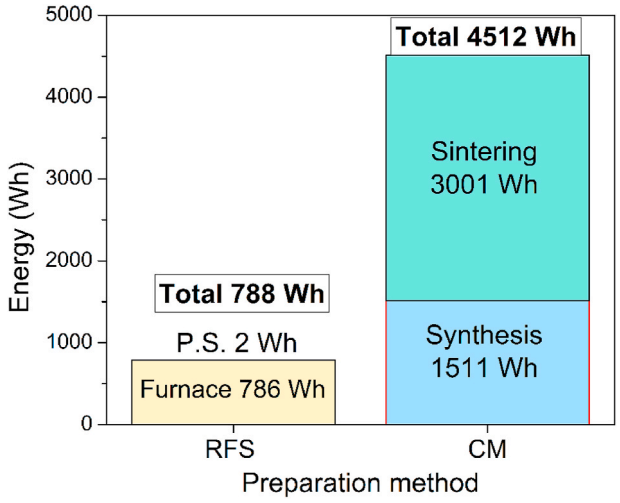

Fig. 9. Electrical energy consumption for the preparation of BFO-33BT by RFS and the conventional method (CM).

Declaration of competing interest

The authors declare that they have no known competing financial interests or personal relationships that could have appeared to influence the work reported in this paper.

Acknowledgements

This work has been supported by the Spanish Government Agency Ministerio de Economía y Competitividad and FEDER (project CTQ2017–83602-C2–1-R) and by Junta de Andalucía-Consejería de Economía, Conocimiento, Empresas y Universidad and FEDER (projects P18-FR-1087 and US-1262507). Financial support from project 201960E092 (INTRAMURAL-CSIC) is also acknowledged. A. Taibi would like also to thank the Direction Générale de la Recherche Scientifique et du Développement Technologique (DGRSDT) of the Algerian Ministry of Higher Education (MESRS) for his PhD scholarship.

References

[1] V.V. Shvartsman, W. Kleemann, R. Haumont, J. Kreisel, Large bulk polarization and regular domain structure in ceramic BiFe O3, Appl. Phys. Lett. 90 (2007), https://doi.org/10.1063/1.2731312.
[2] D. Maurya, H. Thota, K.S. Nalwa, A. Garg, BiFeO3 ceramics synthesized by mechanical activation assisted versus conventional solid-state-reaction process: a comparative study, J. Alloys Compd. 477 (2009) 780–784, https://doi.org/10.1016/j.jallcom.2008.10.155.
[3] D. Wang, G. Wang, S. Murakami, Z. Fan, A. Feteira, D. Zhou, S. Sun, Q. Zhao, I. M. Reaney, BiFeO3-BaTiO3: a new generation of lead-free electroceramics, J. Adv. Dielectr. 8 (2018), https://doi.org/10.1142/S2010135X18300049.
[4] M.M. El-Desoky, M.M. Mostafa, M.S. Ayoub, M.A. Ahmed, Transport properties of Ba-doped BiFeO3 multiferroic nanoparticles, J. Mater. Sci. Mater. Electron. 26 (2015) 6793–6800, https://doi.org/10.1007/s10854-015-3291-x.
[5] J.W. Woo, S.B. Baek, T.K. Song, M.H. Lee, J.U. Rahman, W.J. Kim, Y.S. Sung, M. H. Kim, S. Lee, Nonstoichiometric effects in the leakage current and electrical properties of bismuth ferrite ceramics, J. Korean Ceram. Soc. 54 (2017) 323–330, https://doi.org/10.4191/kcers.2017.54.4.04.
[6] M.H. Lee, D.J. Kim, H.I. Choi, M. Kim, T.K. Song, W. Kim, J.S. Park, D. Do, Low sintering temperature for lead-free BiFeO $_3$ -BaTiO $_3$ ceramics with high piezoelectric performance, J. Am. Ceram. Soc. 102 (2018), https://doi.org/10.1111/jace.16126 jace.16126.
[7] M. Habib, M.H. Lee, D.J. Kim, H.I. Choi, M.H. Kim, W.J. Kim, T.K. Song, Phase evolution and origin of the high piezoelectric properties in lead-free BiFeO3–BaTiO3 ceramics, Ceram. Int. 46 (2020) 22239–22252, https://doi.org/10.1016/j.ceramint.2020.05.301.
[8] K. Tong, C. Zhou, Q. Li, J. Wang, L. Yang, J. Xu, G. Chen, C. Yuan, G. Rao, Enhanced piezoelectric response and high-temperature sensitivity by site-selected doping of BiFeO3-BaTiO3 ceramics, J. Eur. Ceram. Soc. 38 (2018) 1356–1366, https://doi.org/10.1016/j.jeurceramsoc.2017.10.023.
[9] D.J. Kim, M.H. Lee, T.K. Song, Comparison of multi-valent manganese oxides (Mn4+, Mn3+, and Mn2+) doping in BiFeO3-BaTiO3 piezoelectric ceramics, J. Eur. Ceram. Soc. 39 (2019) 4697–4704, https://doi.org/10.1016/j.jeurceramsoc.2019.07.013.
[10] D. Fu, Z. Ning, D. Hu, J. Cheng, F. Wang, J. Chen, Large and temperature-insensitive piezoelectric strain in xBiFeO3–(1−x)Ba(Zr0.05Ti0.95)O3 lead-free piezoelectric ceramics, J. Mater. Sci. 54 (2019) 1153–1161, https://doi.org/10.1007/s10853-018-2926-8.
[11] G.W. Pabst, L.W. Martin, Y.H. Chu, R. Ramesh, Leakage mechanisms in BiFe O3 thin films, Appl. Phys. Lett. 90 (2007), 072902, https://doi.org/10.1063/1.2535663.
[12] S. Cheng, B.P. Zhang, L. Zhao, K.K. Wang, Enhanced insulating and piezoelectric properties of 0.7BiFeO3-0.3BaTiO3 lead-free ceramics by optimizing calcination temperature: analysis of Bi3+ volatilization and phase structures, J. Mater. Chem. C. 6 (2018) 3982–3989, https://doi.org/10.1039/c8tc00329g.
[13] Q. Zheng, L. Luo, K.H. Lam, N. Jiang, Y. Guo, D. Lin, Enhanced ferroelectricity, piezoelectricity, and ferromagnetism in Nd-modified BiFeO3-BaTiO3 lead-free ceramics, J. Appl. Phys. 116 (2014) 184101, https://doi.org/10.1063/1.4901198.
[14] B. Xun, A. Song, J. Yu, Y. Yin, J.F. Li, B.P. Zhang, Lead-free BiFeO3-BaTiO3Ceramics with high Curie temperature: fine compositional tuning across the phase boundary for high piezoelectric charge and strain coefficients, ACS Appl. Mater. Interfaces 13 (2021) 4192–4202, https://doi.org/10.1021/acsami.0c20381.
[15] M.D. Hayat, E. Carlstrom, Electric Field Assisted Sintering of Metal Oxides, 2011. https://odr.chalmers.se/handle/20.500.12380/149151. (Accessed 29 March 2021).
[16] L.B. Caliman, R. Bouchet, D. Gouvea, P. Soudant, M.C. Steil, Flash sintering of ionic conductors: the need of a reversible electrochemical reaction, J. Eur. Ceram. Soc. 36 (2016) 1253–1260, https://doi.org/10.1016/j.jeurceramsoc.2015.12.005.
[17] A.L.G. Prette, M. Cologna, V. Sglavo, R. Raj, Flash-sintering of Co2MnO4 spinel for solid oxide fuel cell applications, J. Power Sources 196 (2011) 2061–2065, https://doi.org/10.1016/j.jpowsour.2010.10.036.
[18] M. Cologna, B. Rashkova, R. Raj, Flash sintering of nanograin zirconia in <5 s at 850°C, J. Am. Ceram. Soc. 93 (2010) 3556–3559, https://doi.org/10.1111/j.1551-2916.2010.04089.x.
[19] S.K. Jha, H. Charalambous, H. Wang, X.L. Phuah, C. Mead, J. Okasinski, H. Wang, T. Tsakalakos, In-situ observation of oxygen mobility and abnormal lattice expansion in ceria during flash sintering, Ceram. Int. 44 (2018) 15362–15369, https://doi.org/10.1016/j.ceramint.2018.05.186.
[20] R. Shi, Y. Pu, W. Wang, Y. Shi, J. Li, X. Guo, M. Yang, Flash sintering of barium titanate, Ceram. Int. 45 (2019) 7085–7089, https://doi.org/10.1016/j.ceramint.2018.12.211.
[21] X. Vendrell, D. Yadav, R. Raj, A.R. West, Influence of flash sintering on the ionic conductivity of 8 mol% yttria stabilized zirconia, J. Eur. Ceram. Soc. 39 (2019) 1352–1358, https://doi.org/10.1016/j.jeurceramsoc.2018.12.048.
[22] X.L. Phuah, J. Cho, T. Tsakalakos, A.K. Mukherjee, H. Wang, X. Zhang, Defects in flash-sintered ceramics and their effects on mechanical properties, MRS Bull. 46 (2021) 44–51, https://doi.org/10.1557/s43577-020-00014-y.
[23] Y. Wu, X. Su, G. An, W. Hong, Dense Na0.5K0.5NbO3 ceramics produced by reactive flash sintering of NaNbO3-KNbO3 mixed powders, Scripta Mater. 174 (2020) 49–52, https://doi.org/10.1016/j.scriptamat.2019.08.035.
[24] R. Shi, Y. Pu, J. Li, X. Guo, W. Wang, M. Yang, Y. Shi, X. Peng, Particle transport mode during flash sintering of sodium bismuth titanate ceramic, Ceram. Int. 45 (2019) 13269–13274, https://doi.org/10.1016/j.ceramint.2019.04.015.
[25] L.A. Perez-Maqueda, E. Gil-Gonzalez, M.A. Wassel, S.K. Jha, A. Perejon, H. Charalambous, J. Okasinski, P.E. Sanchez-Jimenez, T. Tsakalakos, Insight into the BiFeO3 flash sintering process by in-situ energy dispersive X-ray diffraction (ED-XRD), Ceram. Int. 45 (2019) 2828–2834, https://doi.org/10.1016/j.ceramint.2018.07.293.
[26] E. Taghaddos, H. Charalambous, T. Tsakalakos, A. Safari, Electromechanical properties of flash sintered BNT-based piezoelectric ceramic, J. Eur. Ceram. Soc. 39 (2019) 2882–2888, https://doi.org/10.1016/j.jeurceramsoc.2019.03.050.
[27] M.A.B. Wassel, L.A. Pérez-Maqueda, E. Gil-Gonzalez, H. Charalambous, A. Perejon, S.K. Jha, J. Okasinski, T. Tsakalakos, Anisotropic lattice expansion determined during flash sintering of BiFeO3 by in-situ energy-dispersive X-ray diffraction, Scripta Mater. 162 (2019) 286–291, https://doi.org/10.1016/j.scriptamat.2018.11.028.
[28] T. Clemenceau, N. Andriamady, P.M.K Kumar, A. Badran, V. Avila, K. Dahl, M. Hopkins, X. Vendrell, D. Marshall, R. Raj, Flash sintering of Li-ion conducting ceramic in a few seconds at 850 °C, Scripta Mater. 172 (2019) 1–5, https://doi.org/10.1016/j.scriptamat.2019.06.038.
[29] E. Gil-González, A. Perejón, P.E. Sánchez-Jiménez, M.J. Sayagués, R. Raj, L. A. Pérez-Maqueda, Phase-pure BiFeO3 produced by reaction flash-sintering of Bi2O3 and Fe2O3, J. Mater. Chem. A. 6 (2018) 5356–5366, https://doi.org/10.1039/c7ta09239c.
[30] Y. Jia, X. Su, Y. Wu, G. Bai, Z. Wang, X. Yan, T. Ai, P. Zhao, Fabrication of lead zirconate titanate ceramics by reaction flash sintering of PbO-ZrO2-TiO2 mixed oxides, J. Eur. Ceram. Soc. 39 (2019) 3915–3919, https://doi.org/10.1016/j.jeurceramsoc.2019.05.044.
[31] B. Yoon, D. Yadav, S. Ghose, R. Raj, Reactive flash sintering: MgO and α-Al $_2$ O $_3$ transform and sinter into single-phase polycrystals of MgAl $_2$ O $_4$, J. Am. Ceram. Soc. 102 (2018), https://doi.org/10.1111/jace.15974 jace.15974.
[32] V. Avila, R. Raj, Reactive flash sintering of powders of four constituents into a single phase of a complex oxide in a few seconds below 700°C, J. Am. Ceram. Soc. 102 (2019) 6443–6448, https://doi.org/10.1111/jace.16625.
[33] V. Avila, B. Yoon, R.R. Ingraci Neto, R.S. Silva, S. Ghose, R. Raj, L.M. Jesus, Reactive flash sintering of the complex oxide Li0.5La0.5TiO3 starting from an

amorphous precursor powder, Scripta Mater. 176 (2020) 78–82, https://doi.org/10.1016/j.scriptamat.2019.09.037.
[34] H. Zhang, W. Jo, K. Wang, K.G. Webber, Compositional dependence of dielectric and ferroelectric properties in BiFeO3-BaTiO3 solid solutions, Ceram. Int. 40 (2014) 4759–4765, https://doi.org/10.1016/j.ceramint.2013.09.020.
[35] A. Pakalniškis, A. Lukowiak, G. Niaura, P. Głuchowski, D.V. Karpinsky, D.O. Alikin, A.S. Abramov, A. Zhaludkevich, M. Silibin, A.L. Kholkin, R. Skaudžius, W. Strek, A. Kareiva, Nanoscale ferroelectricity in pseudo-cubic sol-gel derived barium titanate - bismuth ferrite (BaTiO3– BiFeO3) solid solutions, J. Alloys Compd. 830 (2020) 154632, https://doi.org/10.1016/j.jallcom.2020.154632.
[36] E. Gil-González, A. Perejón, P.E. Sánchez-Jiménez, D. Román-González, L.A. Pérez-Maqueda, Control of experimental conditions in reaction flash-sintering of complex stoichiometry ceramics, Ceram. Int. 46 (2020) 29413–29420, https://doi.org/10.1016/j.ceramint.2020.05.091.
[37] R. Raj, Joule heating during flash-sintering, J. Eur. Ceram. Soc. 32 (2012) 2293–2301, https://doi.org/10.1016/j.jeurceramsoc.2012.02.030.
[38] R. Raj, A. Kulkarni, J.M. Lebrun, S. Jha, Flash sintering: a new frontier in defect physics and materials science, MRS Bull. 46 (2021) 36–43, https://doi.org/10.1557/s43577-020-00011-1.
[39] Y. Yin, Y. Tang, W. Pan, A. Song, J. Yu, B. Zhang, Relaxor behaviors enhance piezoelectricity in lead-free BiFeO3-BaTiO3 ceramics incorporated with a tiny amount of Bi(Mg1/2Ti1/2)O3 near the morphotropic phase boundary, Ceram. Int. 47 (2021) 9486–9494, https://doi.org/10.1016/j.ceramint.2020.12.082.
[40] H. Yang, C. Zhou, X. Liu, Q. Zhou, G. Chen, W. Li, H. Wang, Piezoelectric properties and temperature stabilities of Mn- and Cu-modified BiFeO3-BaTiO3 high temperature ceramics, J. Eur. Ceram. Soc. 33 (2013) 1177–1183, https://doi.org/10.1016/j.jeurceramsoc.2012.11.019.
[41] Q. Li, J. Wei, T. Tu, J. Cheng, J. Chen, Remarkable piezoelectricity and stable high-temperature dielectric properties of quenched BiFeO $_3$ -BaTiO $_3$ ceramics, J. Am. Ceram. Soc. 100 (2017) 5573–5583, https://doi.org/10.1111/jace.15079.
[42] H. Bouzidi, H. Chaker, M. Es-souni, C. Chaker, H. Khemakhem, Structural, Raman, ferroelectric and magnetic studies of the (1-x)BF-xBCT multiferroic system, J. Alloys Compd. 772 (2019) 877–884, https://doi.org/10.1016/j.jallcom.2018.09.105.
[43] H. Qi, A. Xie, A. Tian, R. Zuo, Superior energy-storage capacitors with simultaneously giant energy density and efficiency using nanodomain engineered BiFeO $_3$ -BaTiO $_3$ -NaNbO $_3$ lead-free bulk ferroelectrics, Adv. Energy Mater. 10 (2020) 1903338, https://doi.org/10.1002/aenm.201903338.
[44] C. Li, T. Zheng, J. Wu, Competitive mechanism of temperature-dependent electrical properties in BiFeO3-BaTiO3 ferroelectrics controlled by domain evolution, Acta Mater. 206 (2021) 116601, https://doi.org/10.1016/j.actamat.2020.116601.
[45] N. Liu, R. Liang, G. Zhang, Z. Zhou, S. Yan, X. Li, X. Dong, Colossal negative electrocaloric effects in lead-free bismuth ferrite-based bulk ferroelectric perovskite for solid-state refrigeration, J. Mater. Chem. C. 6 (2018) 10415–10421, https://doi.org/10.1039/c8tc04125c.
[46] S. Shankar, I. Maurya, A. Raj, S. Singh, O.P. Thakur, M. Jayasimhadri, Dielectric and tunable ferroelectric properties in BiFeO3–BiCoO3–BaTiO3 ternary compound, Appl. Phys. Mater. Sci. Process 126 (2020) 686, https://doi.org/10.1007/s00339-020-03872-0.
[47] A. Singh, A. Kumar, D. Pandey, Effect of synthesis route on structure and dielectric properties of (1-x)BiFeO 3 -xBaTiO 3 solid solutions and its phase diagram, J. Appl. Phys. 124 (2018) 224101, https://doi.org/10.1063/1.5043164.
[48] C. Ji, T. Fan, G. Chen, X. Bai, J. Wang, J. He, W. Cai, R. Gao, X. Deng, Z. Wang, X. Lei, C. Fu, Influence of sintering method on microstructure, electrical and magnetic properties of BiFeO3–BaTiO3 solid solution ceramics, Mater. Today Chem. 20 (2021) 100419, https://doi.org/10.1016/j.mtchem.2020.100419.
[49] S. Murakami, N.T.A.F. Ahmed, D. Wang, A. Feteira, D.C. Sinclair, I.M. Reaney, Optimising dopants and properties in BiMeO3 (Me = Al, Ga, Sc, Y, Mg2/3Nb1/3, Zn2/3Nb1/3, Zn1/2Ti1/2) lead-free BaTiO3-BiFeO3 based ceramics for actuator applications, J. Eur. Ceram. Soc. 38 (2018) 4220–4231, https://doi.org/10.1016/j.jeurceramsoc.2018.05.019.
[50] G. Wang, J. Li, X. Zhang, Z. Fan, F. Yang, A. Feteira, D. Zhou, D.C. Sinclair, T. Ma, X. Tan, D. Wang, I.M. Reaney, Ultrahigh energy storage density lead-free multilayers by controlled electrical homogeneity, Energy Environ. Sci. 12 (2019) 582–588, https://doi.org/10.1039/c8ee03287d.
[51] Q. Li, J. Cheng, J. Chen, Reduced dielectric loss and enhanced piezoelectric properties of Mn modified 0.71BiFeO 3-0.29BaTiO 3 ceramics sintered under oxygen atmosphere, (n.d.). https://doi.org/10.1007/s10854-016-5670-3.
[52] X.Z. Deng, L.Y. Zhang, X.Y. Geng, J. Zhang, L. Sun, R.X. Wang, Z. Bin Gu, S. T. Zhang, Crystal structure, impedance, and multiferroic property of SrZrO3 and MnO2 modified 0.725BiFeO3−0.275BaTiO3 ceramics, Ceram. Int. 43 (2017) 14748–14755, https://doi.org/10.1016/j.ceramint.2017.07.215.
[53] J. Li, J. Cho, J. Ding, H. Charalambous, S. Xue, H. Wang, X.L. Phuah, J. Jian, X. Wang, C. Ophus, T. Tsakalakos, R. Edwin García, A.K. Mukherjee, N. Bernstein, C. Stephen Hellberg, H. Wang, X. Zhang, Nanoscale stacking fault–assisted room temperature plasticity in flash-sintered TiO2, Sci. Adv. 5 (2019), https://doi.org/10.1126/sciadv.aaw5519 eaaw5519.
[54] S. Huo, S. Yuan, Z. Tian, C. Wang, Y. Qiu, Grain size effects on the ferroelectric and piezoelectric properties of Na 0.5K 0.5NbO 3 ceramics prepared by pechini method, J. Am. Ceram. Soc. 95 (2012) 1383–1387, https://doi.org/10.1111/j.1551-2916.2011.04992.x.
[55] D. Wang, Z. Fan, W. Li, D. Zhou, A. Feteira, G. Wang, S. Murakami, S. Sun, Q. Zhao, X. Tan, I.M. Reaney, High energy storage density and large strain in Bi(Zn2/3Nb1/3)O3-doped BiFeO3-Ba"3 ceramics, ACS Appl. Energy Mater. 1 (2018) 4403–4412, https://doi.org/10.1021/acsaem.8b01099.